Int. J. Nonlinear Anal. Appl. 9 (2018) No. 1, 175-193
ISSN: 2008-6822 (electronic)
http://dx.doi.org/10.22075/ijnaa.2017.10429.1502

Investigation of fully developed flow and heat transfer through n-sided polygonal ducts with round corners using the Galerkin weighted residual method

Ali Akbar Abbasian Arani, Ali Arefmanesh, Amirhossein Niroumand*

Department of Mechanical Engineering, Faculty of Mechanical Engineering, University of Kashan, Kashan 87317-51167, Iran

(Communicated by M.B. Ghaemi)

Abstract

The Galerkin weighted residuals method is extended solve the laminar, fully developed flow and heat transfer of Al_2O_3–water nanofluid inside polygonal ducts with round corners for the constant heat flux and uniform wall temperature boundary conditions. Using the method, semi–analytical, closed–form solutions are obtained for the friction coefficient and the Nusselt number in terms of the radius of the round corners for the triangular, rectangular, hexagonal, and octagonal ducts. The effects of varying the radius of the round corners and the volume fraction of the nanoparticles on the friction coefficient and the Nusselt number are analyzed. The results show that the friction factor and the average Nusselt number increase with increasing the radius of the round corners. The study indicates that the Galerkin weighted residuals method is an accurate and efficient technique to obtain closed–form solutions for the flow and temperature fields in ducts with complex cross–sectional shapes.

Keywords: fully developed flow; polygonal ducts; semi-analytic solutions; Galerkin weighted residual method; nanofluid.

2010 MSC: Primary 26A25; Secondary 39B62.

Nomenclature

α *thermal diffusivity,* m^2/s

*Corresponding author
Email addresses: abbasian@kashanu.ac.ir (Ali Akbar Abbasian Arani), arefmanesh@gmail.com (Ali Arefmanesh), ahnmechanics@gmail.com (Amirhossein Niroumand)

Received: February 2017 *Revised:* August 2017

Δp	*pressure drop,* N/m^2
μ	*dynamic viscosity,* $N.s/m^2$
Ω	*solution domain*
$\partial\Omega$	*solution domain boundary*
ϕ	*volume fraction of nanoparticles*
ρ	*density,* kg/m^3
$\sim$	*Approximate value*
θ	*dimensionless temperature*
υ	*kinematics viscosity,* m^2/s
A	*cross-sectional Areas,* m^2
c_p	*specific heat at constant pressure,* $J/Kg.K$
f	*friction factor*
h	*heat transfer coefficient,* $W/m^2.K$
k	*thermal conductivity,* $W/m.K$
L	*length,* m
m	*bulk*
n	*number of sides of polynomial ducts*
nf	*fnanofluid*
Nu	*Nusselt number*
P	*wetted perimeter,* m
p	*pressure,* N/m^2
Q	*heat flux per unit length,* W/m
R_c	*dimensionless round corner radius*
r_c	*round corner radius,* m
Re	*Reynolds number*
s	*nanoparticles*
T	*temperature*
U	*average axial velocity,* m/s

v_x	*axial velocity component, m/s*
w	*weight function*
$\hat{e}_1, \hat{e}_2, \hat{e}_3$	*unit vectors along coordinates*

1. Introduction

Study of the laminar forced convection fluid flow and heat transfer in non–circular ducts is of pre–eminent importance in designing compact heat exchangers, refrigeration and air–conditioning applications and microfluidic devices to mention a few. The essential criteria for designing the duct geometries in compact heat exchangers are possessing a large heat transfer surface to volume ratio, a high heat transfer coefficient, and a corresponding low pressure drop. For polygonal ducts, the heat transfer surface to volume ratio decreases with increasing the number of sides. From this standpoint, a triangular duct is the most preferred one; while, a circular duct is the least desirable duct geometry. Rounding the corners of these ducts is also a means of improving their heat transfer performance. However, one should bear in mind that providing the maximum possible heat transfer coefficient is not the solitary criterion for selecting the duct geometry. Undoubtedly, having a low value of the friction factor is another crucial objective of compact heat exchanger designers. Therefore, the study of fluid flow and heat transfer in the polygonal ducts with round corners seems to be essential for designing compact heat exchangers.

As far as semi–analytical solutions for fluid flow through ducts are concerned, Sparrow and Siegel [1], Sparrow and Loeffler [2] and Sparrow et al. [3] are among the first investigators who obtained approximate closed–form solutions for fluid flow and heat transfer through rectangular and circular sector ducts using a variational method. Using this method, Cheng and Jamil [4] solved the laminar flow and heat transfer in the circular ducts with diametrically opposite flat sides and in the ducts of multiply connected cross–sections. Sparrow and Haji–Sheikh [5] and Ratrowsky and Epstein [6] used another semi–analytical technique, i.e., least squares point–matching method, with the Gram–Schmidt orthogonalization procedure to analyze the fully developed laminar fluid flow and heat transfer in ducts of arbitrary cross-sectional shapes. However, they provided results for ducts of circular–segment cross-sections only. Subsequently, Shah [7] employed an improved version of the least square point–matching technique, using a computationally fast and more accurate least–squares approximation due to Golub [8], to analyze the fully developed laminar fluid flow and heat transfer in ducts of arbitrary cross–sections under the constant axial heat flux boundary condition. Haji–Sheikh et al. [9] and Lee and Kuo [10] used the Galerkin integral method to obtain closed–form solutions for the heat transfer through non–circular ducts. Using a similar method, Lee and Lee [11] obtained closed–form solutions for the laminar, fully developed flow in elliptical ducts with and without central circular cores. Tehernejad Ledari et al. [12] utilized a semi analytical Akbari Ganji's Method (AGM) to solve two–dimension nonlinear viscous flow between slowly expanding or contracting walls. They found that AGM could be applicable through other methods in nonlinear problems with high nonlinearity.

As far as recent semi–analytical studies regarding the fluid flow and heat transfer through ducts of non–circular cross–section are concerned, Ray and Misra [13] employed the least squares point–matching technique to investigate the laminar, fully developed flow through square and equilateral triangular ducts with round corners for two types of boundary conditions, namely, constant axial heat input and uniform peripheral wall temperature, and uniform axial, as well as, peripheral heat

input. They concluded that the friction factor and effectiveness of the round portion for both of the considered duct geometries increased rapidly with increasing the radius of the round corners. In another very recent study, Shahsavari et al. [14] employed the least squares point–matching technique to obtain closed–form solutions for fluid flow in micro/mini–channels. They proposed two correlations for the friction coefficient and the Nusselt number for regular polygonal ducts with sharp corners. A considerable number of numerical studies, employing the finite difference, finite element, and finite volume methods, devoted to the solutions of the velocity and temperature fields in the laminar, fully developed flow through non–circular ducts are available in the literature [15, 16, 17, 18, 19, 20, 21, 22]. Among very recent studies in this category are the numerical investigation of Turgut [23] who considered laminar flow and heat transfer in hexagonal ducts under isothermal and constant heat flux boundary conditions and that of Ebaid et al. [24] who analyzed the fully developed laminar flow in irregular annulus ducts. There are also a number of very recent numerical as well as experimental studies regarding the use of nanofluid on the fluid flow and heat transfer through ducts (Zeinali Heris et al. [25]; Vajjha et al. [26]; Nassan et al. [27]; Kumar [28]; Nasiri et al. [29]; Zeinali Heris et al. [30]; Dawood et al. [31]). Evidently, semi–analytical closed–form solution for the above cases, whenever possible, are preferred to the numerical ones which provide the values of the velocity and temperature fields at the nodes of a mesh only. The above literature survey indicate that, even though there exist some semi–analytical results obtained mainly by using the least square point–matching technique for the laminar, fully developed flow of fluids through ducts with complex geometries, the performance of the Galerkin weighted residuals method to obtain approximate closed–form solution for non–isothermal fluid flow through ducts with complex cross–sections, such as polygonal cross–sections with round corners, for different possible boundary conditions remains to be explored. Therefore in this study, the Galerkin weighted residual method is extended to solve the laminar fully developed fluid flow and heat transfer of Al_2O_3–water nanofluid inside polygonal ducts with round corners for two types of temperature boundary conditions, namely, the constant axial heat flux and uniform peripheral wall temperature, and the uniform temperature both axially and peripherally. Using this method, semi–analytical closed–form solutions are obtained and presented for the friction coefficient and the Nusselt number for the n–sided polygonal ducts in terms of the radius of the round corners and the volume fraction of nanoparticles. Furthermore, the impacts of the curvature of the round corners and the volume fraction of the nanoparticles on the pressure drop and heat transfer are explored.

2. Mathematical formulation

The following analysis is concerned with the hydrodynamically and thermally fully developed, laminar fluid flow and heat transfer of Al_2O_3–water nanofluid through regular n–sided polygonal ducts with round corners. In this section, the governing equations and the boundary conditions are briefly presented and discussed, and in the subsequent section, their solutions by the Galerkin weighted residuals method are demonstrated

2.1. Problem Geometry

A schematic of a representative regular polygonal (hexagonal) duct with round corners and the associated coordinate system are depicted in Fig. 1 (a). As it is observed from this figure, the nanofluid enters the duct with a uniform axial velocity U and a uniform temperature Tin. The geometrical details for the duct cross–section are shown in Fig. 1 (b). The solution domain and its boundary are designated as Ω and $\partial\Omega$, respectively. The length of the side and the radius of round corners for the regular hexagonal cross–section are denoted by a and r_c, respectively (Fig. 1 (b)).

Table 1: Hydraulic diameters of the considered duct cross-sections

Cross section	D_h
Triangle	$a/\sqrt{3}$
Square	a
Hexagon	$a\sqrt{3}$
Octagon	$\sqrt{2\left(3/2+\sqrt{2}\right)}a$

Figure 2 depicts the geometrical details of the solution domains for different duct cross–sections which are considered in the present analysis. The dimensionless radius of the round corners for these ducts is defined as $R = r_c/a$. For the duct cross–sections shown in Fig. 2, R_c can vary from a minimum to a maximum value. The minimum value of R_c, which is equal to zero for all of the considered duct cross-sections, corresponds to the sharp–cornered ducts. The maximum value of R_c for the triangular, square, hexagonal, and octagonal ducts shown in Fig. 2, which is equal to the dimensionless radius of the corresponding inscribed circle for each case, is $1/\sqrt{3}$, 1, 0.866, and 1.207, respectively. Through varying R_c from the minimum to the maximum values, a family of round corner ducts can be generated for each of the duct geometries depicted in Fig. 2.

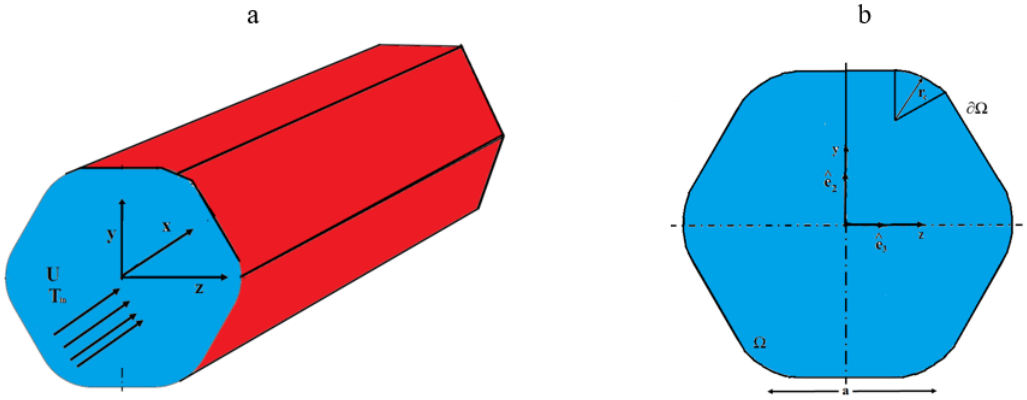

Figure 1: (a) Geometry and coordinate system for the regular 6–sided polygonal duct. (b) Details of the cross–section of the duct.

The hydraulic diameter for the duct cross–section is defined as

$$D_h = \frac{4A}{P}, \tag{2.1}$$

where A is the cross–sectional area of the duct, and P denotes its wetted perimeter. The hydraulic diameters for the considered duct cross–sections shown in Fig. 1 are presented in Table 1.

2.2. Governing Equation

In this section, the equations governing the hydrodynamically and thermally fully developed flow of the nanofluid through ducts are briefly presented.

2.2.1. Governing Momentum Equation

The only non–zero velocity component in the hydrodynamically fully developed region of the duct shown in Fig.1 is the axial component $v_x = v_x(y, z)$. The governing momentum equation for the

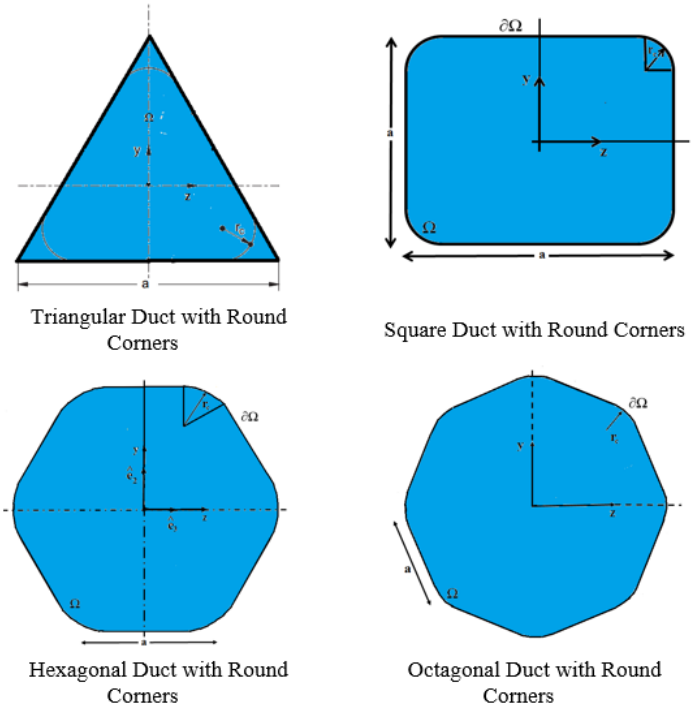

Figure 2: Coordinate system and the geometrical details of the considered regular, polygonal duct cross–sections.

axial direction is given by

$$\mu_{nf}\left(\frac{\partial^2 v_x}{\partial y^2}+\frac{\partial^2 v_x}{\partial z^2}\right)=\frac{dp}{dx}, \tag{2.2}$$

where dp/dx is the axial pressure gradient which has a constant value for the hydrodynamically fully developed flow and for a fixed nanoparticles volume fraction. As far as boundary condition for Eq. (2.2) is concerned, the essential no–slip boundary condition $v_x = 0$ is imposed along $\partial\Omega$ (Fig. 1 (b)). Solving Eq. (2.2) with the aforementioned boundary condition yields the axial velocity component in terms of dp/dx and the viscosity of the nanofluid.

The axial pressure gradient dp/dx, for a fixed nanoparticles volume fraction in the fully developed region is equal to $\Delta p/L$ where Δp is the pressure drop along length L of the duct. The pressure drop Δp can be calculated from the following formula:

$$\Delta p=\frac{2fL}{D_h}\left(\rho_f U^2\right). \tag{2.3}$$

Subsequent to solving the momentum equation, Eq. (2.2), the average axial velocity component U for the incompressible nanofluid can be calculated from the following equation in terms of the constant pressure gradient:

$$AU=\int_\Omega v_x dydz, \tag{2.4}$$

where A is the area of the duct cross–section. Substituting the resulting average velocity from Eq. (2.4) into Eq. (2.3) yields the value of the friction factor f.

2.2.2. Governing Energy Equation

As far as the heat transfer to the fully developed duct flow is concerned, the scale analysis shows that, in the hydrodynamically and thermally fully developed region in the limit of large Peclet numbers, the axial conduction effect is negligible compared to the convection heat transfer, and the Nusselt number has a constant value of order one Bejan [32]. Moreover, the only non–zero velocity component in this region of the duct is $v_x = v_x(y, z)$. Consequently, under such circumstances, the energy equation simplifies to

$$\frac{v_x\left(y,z\right)}{\alpha_{nf}}\frac{\partial T}{\partial x}=\frac{\partial^2 T}{\partial y^2}+\frac{\partial^2 T}{\partial z^2}, \tag{2.5}$$

where α_{nf} is the thermal diffusivity of the nanofluid. A scale analysis conducted by Bejan [32] shows that in the hydrodynamically and thermally fully developed region of tube, the Nusselt number is a constant of order one. Moreover, he has demonstrated that an immediate consequence of the Nusselt number being a constant of order one is that the dimensionless temperature does not vary along the axial direction of the duct in the fully developed region [32]. Consequently, the dimensionless fully developed temperature is written as [32]

$$\frac{T_w\left(x\right)-T\left(x,y,z\right)}{T_w\left(x\right)-T_m\left(x\right)}=\theta\left(y,z\right), \tag{2.6}$$

where $T_m(x)$ is the bulk temperature of the stream which is defined as

$$T_m=\frac{1}{\rho_{nf}AU}\int_{A_\Omega}\rho_{nf}v_xTdydz, \tag{2.7}$$

where ρ_{nf} is the density of nanofluid. Choosing the temperature profile obtained by Eq. (2.6) asserts that the fluid flow is thermally fully developed. Applying the First Law of Thermodynamics to the fully developed duct flow yields ([32])

$$\frac{dT_m}{dx}=\frac{q}{\left(\rho c_p\right)_{nf}AU}. \tag{2.8}$$

Two types of the wall–temperature boundary conditions, namely **H1** (i.e., constant axial heat flux and uniform peripheral wall temperature) and T (i.e., uniform temperature both axially and peripherally) boundary conditions, are considered in the current analysis. It should be noted that the results presented in reference [13] using the least–squares point–matching technique do not include the **T** boundary condition. For the **H1** boundary condition, q and consequently dTm/dx in Eq. (2.8) have constant values for a fixed nanoparticles volume fraction. The heat transfer per unit duct length is given by

$$q=hP\left(T_w-T_m\right), \tag{2.9}$$

where h is the average heat transfer coefficient which is constant in the fully developed region. Employing Eq. (2.9), the fully developed temperature profile Eq. (2.6) is reduced to

$$T\left(x,y,z\right)=T_w\left(x\right)-\frac{q}{hP}\theta\left(y,z\right). \tag{2.10}$$

It is concluded from the above equation that $\partial T/\partial x = dTm/dx$. Moreover, a consequence of Nu_{Dh} having a constant value of order one is that $dTw/dx = dTm/dx$. Therefore, the derivative of the temperature along the axial direction can be written as

$$\frac{\partial T}{\partial x} = \frac{q}{(\rho c_p)_{nf} AU}. \tag{2.11}$$

Substituting the temperature profile (2.10) and $\partial T/\partial x$ from (2.11) into Eq. (2.5) leads to the following equation for θ for the **H1** boundary condition:

$$\frac{k_f}{k_{nf}} \frac{4v_x}{UD_h^2} Nu_{D_h} = -\left(\frac{\partial^2 \theta}{\partial y^2} + \frac{\partial^2 \theta}{\partial z^2}\right). \tag{2.12}$$

The boundary condition to be imposed on θ is given by

$$\theta = 0 \ \text{ on } \ \partial\Omega\,, \tag{2.13}$$

which is a direct consequence of the temperature being equal to T_w at the duct wall.

For the **T** boundary condition, the temperature of the duct wall is uniform both axially and peripherally, i.e., $T_w = constant$. Hence, it is concluded from (2.6) that $\partial T/\partial x = dTm/dx$. Using Eqs. (2.8) and (2.9), this latter relation can be written as

$$\frac{\partial T}{\partial x} = \frac{4Nu_{D_h}\alpha_{nf}}{UD_h^2} \frac{k_f}{k_{nf}} (T_w - T_m)\,\theta. \tag{2.14}$$

Substituting the temperature profile (2.6) for the case of T_w being constant, and $\partial T/\partial x$ from Eq. (2.14) into Eq. (2.5) leads to the following equation for θ for the **T** boundary condition:

$$\frac{\partial^2 \theta}{\partial y^2} + \frac{\partial^2 \theta}{\partial z^2} = \frac{k_f}{k_{nf}} \frac{4Nu_{D_h}}{UD_h^2} v_x \theta. \tag{2.15}$$

The boundary condition for Eq. (2.15) is the same as that given in (2.13).

2.3. Thermophysical Properties of Nanofluids

The primary purpose of the present investigation is to develop closed–form solutions for the fully developed flow and temperature fields for a nanofluid flowing through the polygonal ducts with round corners employing the Galerkin weighted residuals method. The Al_2O_3–water nanofluid is employed for this purpose due to its widespread application and well–established thermophysical properties. A number of constant and variable-property models are available for the thermophysical properties of the nanofluid [33]. The thermophysical properties of the nanofluid in the constant–property models are function of the nanoparticles, and in the variable–property models depend on both the volume fraction of the nanoparticles and the temperature. However, as it has been demonstrated theoretically by Bejan [32] and numerically by other investigators [34], the effect of the temperature on the thermophysical properties of an incompressible flow is not significant. Moreover, employing variable–property models for the nanofluid in the present study makes the solution procedure complicated as a result of requiring iterative solution scheme. Hence, the constant–property thermophysical models for Al_2O_3–water nanofluid based on the experimental results are employed in the current analysis.

The thermophysical properties of water and Al_2O_3 nanoparticles are given in Table 2. The density and the heat capacity of the nanofluid are obtained from the following relations, respectively:

$$\rho_{nf} = (1-\phi)\,\rho_f + \phi\rho_s \tag{2.16}$$

and

$$(\rho c_p)_{nf} = (1-\phi)(\rho c_p)_f + \phi(\rho c_p)_s. \tag{2.17}$$

The effective thermal conductivity of the nanofluid, which is obtained from the models proposed by Yu and choi [35], is given by:

$$\frac{k_{nf}}{k_f} = \frac{k_s + 2k_f + 2\phi(k_s - k_f)(1+\beta)^3}{k_s + 2k_f - \phi(k_s - k_f)(1+\beta)^3}, \tag{2.18}$$

where β=0.1. The thermal diffusivity of the nanofluid is obtained from $\alpha_{nf} = k_{nf}/(\rho c_p)_{nf}$. The effective viscosity for the nanofluid is calculated from the following relation proposed by Maiga et al. [36]:

$$\frac{\mu_{nf}}{\mu_f} = 1 + 7.3\phi + 123\phi^2. \tag{2.19}$$

Table 2: Thermophysical properties of water and Al_2O_3 nanoparticles.

Physical properties	$c_p\,(Jkg^{-1}K^{-1})$	$\rho\,(kgm^{-3})$	$k\,(Wm^{-1}K^{-1})$	$\mu\,(kgm^{-1}s^{-1})$
Water	4179	997.1	0.613	9.93×10^{-4}
Nanoparticles(Al_2O_3)	765	3970	25	-

3. Galerkin Weighted Residuals formulations

The governing equations for the hydrodynamically and thermally fully developed flow of the nanofluid through ducts for the **H1** and the T wall–temperature boundary conditions are Eqs. (2.2) and (2.12), and Eqs. (2.2) and (2.15), respectively. These equations cannot be solved analytically for the complex duct geometries shown in Fig. 2. A number of numerical methods, such as, the finite element method and the finite difference, can be utilized for this purpose. However, in this section, the Galerkin weighted residuals method is employed to obtain approximate, closed–form solutions for the fully developed flow and temperature fields of the ducts depicted in Fig. 2. The semi–analytic solutions obtained using this method is superior compared to the numerical solutions. For example, the geometrical procedures, such as the radius of the round corners, and the nanofluid properties can be easily changed in the closed form solutions without requiring further computations; however, remeshing of the solution domain and solving the governing equations over the new mesh are required with changing these parameters while using numerical techniques.

In this section, the Galerkin weighted residuals method is employed to obtain approximate, closed–form solutions for these equations for the ducts depicted in Fig. 2. Details of the Galerkin weighted residuals solution method implementation are subsequently presented for the hexagonal duct cross–section shown in Fig. 1 (b) as a representative of the n-sided regular polygonal ducts considered in the current study.

3.1. Galerkin weighted Residuals method for velocity field

To solve the velocity field in the domain Ω shown in Fig. 1 (b) by the method of weighted residuals, an approximate solution $v_x \approx \tilde{v}_x(y,z)$ is sought of the form

$$\tilde{v}_x(y,z) = \left[y + \sqrt{3}(z-a)\right]\left[y - \sqrt{3}(z+a)\right]\left[y + \sqrt{3}(z+a)\right]\left[y - \sqrt{3}(z-a)\right] \tag{3.1}$$

$$\left(y-\frac{\sqrt{3}}{2}a\right)\left(y+\frac{\sqrt{3}}{2}a\right)\left\{\left[z-\left(a-\frac{2R_c}{\sqrt{3}}\right)\right]^2-y^2-{R_c}^2\right\}$$
$$\left\{\left[z-\left(\frac{a}{2}-\frac{R_c}{\sqrt{3}}\right)\right]^2-\left[y-\left(\frac{\sqrt{3}}{2}a-R_c\right)\right]^2-{R_c}^2\right\}$$
$$\left\{\left[z-\left(\frac{R_c}{\sqrt{3}}-\frac{a}{2}\right)\right]^2-\left[y-\left(\frac{\sqrt{3}}{2}a-R_c\right)\right]^2-{R_c}^2\right\}$$
$$\left\{\left[z-\left(\frac{2R_c}{\sqrt{3}}-a\right)\right]^2-y^2-{R_c}^2\right\}$$
$$\left\{\left[z-\left(\frac{R_c}{\sqrt{3}}-\frac{a}{2}\right)\right]^2-\left[y-\left(R_c-\frac{\sqrt{3}}{2}a\right)\right]^2-{R_c}^2\right\}$$
$$\left\{\left[z-\left(\frac{a}{2}-\frac{R_c}{\sqrt{3}}\right)\right]^2-\left[y-\left(R_c-\frac{\sqrt{3}}{2}a\right)\right]^2-{R_c}^2\right\}\left(\sum_{i,j=0}^{i+j\le m_v}c_{ij}y^iz^j\right),$$

where the expressions inside the first twelve brackets in the right–hand side of Eq. (3.1), when separately equated to zero, yield the respective equations for different segments of the boundary $\partial\Omega$ (Fig. 1 (b)), and m_v denotes the order of the complete polynomial in two-space dimension in the last bracket. $c_{ij}, 0\le i+j\le m_v$ in Eq. (3.1) are unknown coefficients. An essential characteristic of the above approximate solution is that it satisfies the no–slip boundary condition on $\partial\Omega$ for all choices of the unknown coefficients. Substituting the above approximate solution into Eq. (2.2) yields in a residual. The unknown coefficients, $c_{ij}, 0\le i+j\le m_v$ are then calculated by setting the weighted integral of the residual to zero

$$\int_\Omega\left[\mu_{nf}\left(\frac{\partial^2\tilde{v}_x}{\partial y^2}+\frac{\partial^2\tilde{v}_x}{\partial z^2}\right)-\frac{dp}{dx}\right]w_{ij}dydz=0\,,\quad 0\le i+j\le m_v. \tag{3.2}$$

In the Galerkin weighted residuals method which is employed in the current study, the following weighting functions are employed:

$$\tilde{w}_{ij}=\left[y+\sqrt{3}\,(z-a)\right]\left[y-\sqrt{3}\,(z+a)\right]\left[y+\sqrt{3}\,(z+a)\right]\left[y-\sqrt{3}\,(z-a)\right]$$
$$\left(y-\frac{\sqrt{3}}{2}a\right)\left(y+\frac{\sqrt{3}}{2}a\right)\left\{\left[z-\left(a-\frac{2r_c}{\sqrt{3}}\right)\right]^2-y^2-{R_c}^2\right\}$$
$$\left\{\left[z-\left(\frac{a}{2}-\frac{R_c}{\sqrt{3}}\right)\right]^2-\left[y-\left(\frac{\sqrt{3}}{2}a-R_c\right)\right]^2-{R_c}^2\right\}$$
$$\left\{\left[z-\left(\frac{R_c}{\sqrt{3}}-\frac{a}{2}\right)\right]^2-\left[y-\left(\frac{\sqrt{3}}{2}a-R_c\right)\right]^2-{R_c}^2\right\} \tag{3.3}$$

$$\left\{\left[z-\left(\frac{2R_c}{\sqrt{3}}-a\right)\right]^2-y^2-{R_c}^2\right\}$$
$$\left\{\left[z-\left(\frac{R_c}{\sqrt{3}}-\frac{a}{2}\right)\right]^2-\left[y-\left(R_c-\frac{\sqrt{3}}{2}a\right)\right]^2-{R_c}^2\right\}$$
$$\left\{\left[z-\left(\frac{a}{2}-\frac{R_c}{\sqrt{3}}\right)\right]^2-\left[y-\left(R_c-\frac{\sqrt{3}}{2}a\right)\right]^2-{R_c}^2\right\}y^i z^j.$$

Substituting the expression (3.1) for $\tilde{v}_x$ into Eq. (3.2) and performing the required integration lead to a system of algebraic equations for the unknown coefficients $c_{ij}, 0 \leq i+j \leq m_v$. The above procedure can be applied to any of the duct cross–sections shown in Fig. 2. However, the factors in front of the last bracket in the right–hand side of (3.1) will be different for different cross–sections. These factors for the considered different cross–sections are given in Table 3.

Following the calculation of the coefficients $c_{ij}, 0 \leq i+j \leq m_v$, the average velocity is obtained from Eq. (2.4) by replacing v_x with the resulting approximate solution for the velocity (Eq. (3.1)). The friction factor f can subsequently be obtained by substituting the calculated average velocity into (2.3), noting that in the fully developed region of the duct dp/dx is equal to $-\nabla p/L$.

3.2. Galerkin weighted Residuals method for velocity field

As far as heat transfer in the fully developed region of the duct is concerned, the partial differential equations (2.12) and (2.15) should be solved to obtain the fully developed temperature profile for the **H1** and the **T** wall–temperature boundary conditions, respectively. In the following, the details of the Galerkin weighted residuals method employed to obtain approximate, closed–form solution for these equations are presented for the hexagonal duct cross–section shown in Fig. 1 (b).

The solution procedure is initiated by seeking an approximate solution $\theta \approx \tilde{\theta}(y,z)$ for the temperature field given by

$$\begin{aligned}
&\phi(y,z)=\left[y+\sqrt{3}(z-a)\right]\left[y-\sqrt{3}(z+a)\right]\left[y+\sqrt{3}(z+a)\right]\left[y-\sqrt{3}(z-a)\right]\\
&\left(y-\frac{\sqrt{3}}{2}a\right)\left(y+\frac{\sqrt{3}}{2}a\right)\left\{\left[z-\left(a-\frac{2R_c}{\sqrt{3}}\right)\right]^2-y^2-{R_c}^2\right\}\\
&\left\{\left[z-\left(\frac{a}{2}-\frac{R_c}{\sqrt{3}}\right)\right]^2-\left[y-\left(\frac{\sqrt{3}}{2}a-R_c\right)\right]^2-{R_c}^2\right\}\\
&\left\{\left[z-\left(\frac{R_c}{\sqrt{3}}-\frac{a}{2}\right)\right]^2-\left[y-\left(\frac{\sqrt{3}}{2}a-R_c\right)\right]^2-{R_c}^2\right\}\\
&\left\{\left[z-\left(\frac{2R_c}{\sqrt{3}}-a\right)\right]^2-y^2-{R_c}^2\right\}\\
&\left\{\left[z-\left(\frac{R_c}{\sqrt{3}}-\frac{a}{2}\right)\right]^2-\left[y-\left(R_c-\frac{\sqrt{3}}{2}a\right)\right]^2-{R_c}^2\right\}\\
&\left\{\left[z-\left(\frac{a}{2}-\frac{R_c}{\sqrt{3}}\right)\right]^2-\left[y-\left(R_c-\frac{\sqrt{3}}{2}a\right)\right]^2-{R_c}^2\right\}\left(\sum_{i,j=0}^{i+j\leq m_v}c_{ij}y^i z^j\right).
\end{aligned}\tag{3.4}$$

Table 3: Factors in front of the last bracket in Eqs. (3.1) and (3.4) for the n-sided regular polygonal duct cross- sections shown in Fig. (2)

Triangular	$\left(y+\sqrt{3}z-\frac{\sqrt{3}}{3}a\right)\left(y-\sqrt{3}z-\frac{\sqrt{3}}{3}a\right)\left(y+\frac{\sqrt{3}}{6}a\right)\left\{\left[y-\left(\frac{a}{\sqrt{3}}-2R_c\right)\right]^2+z^2-{R_c}^2\right\}$
	$\left\{\left[y-\left(R_c-\frac{a}{2\sqrt{3}}\right)\right]^2+\left[z-\left(R_c\sqrt{3}-\frac{a}{2}\right)\right]^2-{R_c}^2\right\}$
	$\left\{\left[y-\left(R_c-\frac{a}{2\sqrt{3}}\right)\right]^2+\left[z-\left(\frac{a}{2}-R_c\sqrt{3}\right)\right]^2-{R_c}^2\right\}$
Square	$\left(z^2-\frac{a^2}{4}\right)\left(y^2-\frac{a^2}{4}\right)\left\{\left[z-\left(\frac{a}{2}-R_c\right)\right]^2-\left[y-\left(\frac{a}{2}-R_c\right)\right]^2-{R_c}^2\right\}$
	$\left\{\left[z-\left(-\frac{a}{2}+R_c\right)\right]^2+\left[y-\left(-\frac{a}{2}+R_c\right)\right]^2-{R_c}^2\right\}$
	$\left\{\left[z-\left(-\frac{a}{2}+R_c\right)\right]^2+\left[y-\left(\frac{a}{2}-R_c\right)\right]^2-{R_c}^2\right\}$
	$\left\{\left[z-\left(\frac{a}{2}-R_c\right)\right]^2+\left[y-\left(-\frac{a}{2}+R_c\right)\right]^2-{R_c}^2\right\}$
Hexagonal	$\left[y+\sqrt{3}\left(z-a\right)\right]\left[y-\sqrt{3}\left(z+a\right)\right]\left[y+\sqrt{3}\left(z+a\right)\right]\left[y-\sqrt{3}\left(z-a\right)\right]$
	$\left(y-\frac{\sqrt{3}}{2}a\right)\left(y+\frac{\sqrt{3}}{2}a\right)\left\{\left[z-\left(a-\frac{2R_c}{\sqrt{3}}\right)\right]^2+y^2-{R_c}^2\right\}$
	$\left\{\left[z-\left(\frac{a}{2}-\frac{R_c}{\sqrt{3}}\right)\right]^2+\left[y-\left(\frac{\sqrt{3}}{2}a-R_c\right)\right]^2-{R_c}^2\right\}$
	$\left\{\left[z-\left(\frac{R_c}{\sqrt{3}}-\frac{a}{2}\right)\right]^2+\left[y-\left(\frac{\sqrt{3}}{2}a-R_c\right)\right]^2-{R_c}^2\right\}$
	$\left\{\left[z-\left(\frac{R_c}{\sqrt{3}}-\frac{a}{2}\right)\right]^2+\left[y-\left(R_c-\frac{\sqrt{3}}{2}a\right)\right]^2-{R_c}^2\right\}$
	$\left\{\left[z-\left(\frac{a}{2}-\frac{R_c}{\sqrt{3}}\right)\right]^2+\left[y-\left(R_c-\frac{\sqrt{3}}{2}a\right)\right]^2-{R_c}^2\right\}$
	$\left\{\left[z-\left(\frac{2R_c}{\sqrt{3}}-a\right)\right]^2+y^2-{R_c}^2\right\}$
Octagonal	$(y+2.414213272z-3.15432165a)\,(y+0.4142136z-1.30652965a)$
	$(y-0.4142136z-1.30652965a)\,(y+2.4142132z+3.15432165a)$
	$(y+2.4142132z+3.15432165a)\,(y+0.4142136z+1.30652965a)$
	$(y-0.4142136z+1.30652965a)\,(y-2.414213272z+3.154321a)$
	$\left\{[z-(0.765429R_c-0.9238795a)]^2+[y-(0.9238795a-0.765429R_c)]^2-{R_c}^2\right\}$
	$\left\{[z-(0.9238795a-0.765429R_c)]^2+[y-(0.9238795a-0.765429R_c)]^2-{R_c}^2\right\}$
	$\left\{[z-(0.765429R_c-0.9238795a)]^2+[y-(0.765429R_c-0.9238795a)]^2-{R_c}^2\right\}$
	$\left\{[z-(0.9238795a-0.765429R_c)]^2+[y-(0.765429R_c-0.9238795a)]^2-{R_c}^2\right\}$
	$\left\{[z-(1.3065629a-1.082392R_c)]^2+y^2-{R_c}^2\right\}$
	$\left\{z^2+[y-(1.3065629a-1.082392R_c)]^2-{R_c}^2\right\}$
	$\left\{[z-(1.082392R_c-1.3065629a)]^2+y^2-{R_c}^2\right\}$
	$\left\{z^2+[y-(1.082392R_c-1.3065629a)]^2-{R_c}^2\right\}$

The above approximate solution, which is similar to Eq. (3.1), satisfies the homogenous boundary condition (Eq.(2.13)) on $\partial\Omega$ irrespective of the values of the unknown constant coefficients $c_{ij}, 0 \leq i+j \leq m_T$. The distinct factors in front of the last bracket in the right–hand side of Eq. (3.4) for the different duct cross–sections shown in Fig. (2) are presented in Table 3. Following a procedure similar to the one which has been employed in section 4.1 for the velocity field, the Galerkin weighted residuals equations for Eqs.(2.12) and (2.15) are, respectively, written as

$$\int\limits_{\Omega}\left(\frac{\partial^2\tilde{\theta}}{\partial y^2}+\frac{\partial^2\tilde{\theta}}{\partial z^2}\right)w_{ij}dydz=\int\limits_{\Omega}\frac{4\tilde{v}_x}{UD_h^2}\frac{k_f}{k_{nf}}Nu_{_{D_h}}w_{ij}dydz\,,\ 0\leq i+j\leq m_T \tag{3.5}$$

and

$$\int\limits_{\Omega}\left(\frac{\partial^2\tilde{\theta}}{\partial y^2}+\frac{\partial^2\tilde{\theta}}{\partial z^2}\right)w_{ij}dydz=\int\limits_{\Omega}\frac{4\tilde{v}_x}{UD_h^2}\frac{k_f}{k_{nf}}Nu_{_{D_h}}w_{ij}\tilde{\theta}dydz,\quad 0\leq i+j\leq m_T, \tag{3.6}$$

where the weighting functions wij are given by Eq. (3.3), with replacing mv with m_T.

For the **H1** wall–temperature boundary condition, the unknown coefficients $c_{ij}, 0 \leq i+j \leq m_T$ are determined by solving the system of algebraic equations which results from substituting the expression Eq. (3.4) for into Eq. (3.5) and performing the required integrations. Subsequently, and the fully developed temperature profile, Eq. (2.6), are obtained in terms of Nu_{Dh} which is yet unknown. Afterwards, Nu_{Dh} is calculated by substituting the resulting fully developed temperature profile into the definition of the bulk temperature of the stream, Eq. (2.7), and simplifying the resulting expression.

For the **T** wall–temperature boundary condition, the system of algebraic equations, which is obtained by substituting the expression (3.4) for into Eq. (3.6) is homogenous. The homogenous system of equations admits nontrivial solutions if and only if the determinant of its coefficients is zero. Setting the determinant to zero leads to a characteristic equation whose solution yields the value of Nu_{Dh}. Subsequently, the coefficients $c_{ij}, 0 \leq i+j \leq m_T$, are calculated, and θ as well as the fully developed temperature profile are obtained.

4. Results and discussion

The hydrodynamically and thermally fully developed flow and heat transfer of the Al_2O_3–water nanofluid through the n–sided regular polygonal ducts with round corners shown in Fig. 2 are analyzed using the Galerkin weighted residual method for the constant heat flux and uniform wall temperature boundary conditions. For each of the considered duct cross–sections, approximate closed–form solutions for the fully developed velocity and temperature profiles are obtained using the proposed method. The result for fRe_{Dh} the Reynolds number based on the hydraulic diameter of the duct is defined as $\mathrm{Re}_{Dh} = \rho D_h U/\mu$ and the average Nusselt number, Nu_{Dh}, for the **H1** and **T** wall–temperature boundary conditions are presented for ϕ=0.0, 0.01, and 0.02. Furthermore, whenever possible the results are compared with the available results from the literature.

Figures 3 (a) and 3 (b) compare the results of the present study for fRe_{Dh} for the triangular and square ducts with round corners (ϕ =0.0) with those of Ray and Misra [13] which have been obtained by the least squares point–matching technique. As it is demonstrated by the figure, very good agreements exist between the present results for the base fluid and those of Ray and Misra [13] for the entire range of values of the dimensionless radius of the round corners.

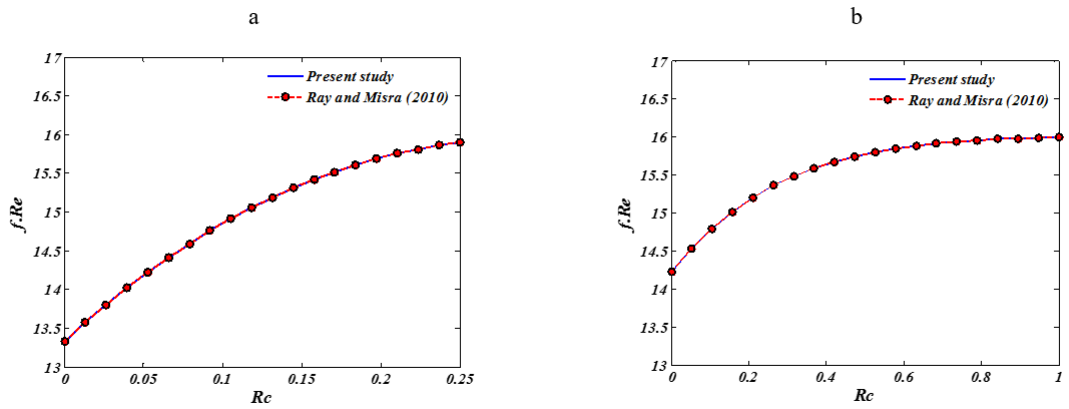

Figure 3: Comparisons between the results of the present study for fRe_{Dh} with those of Ray and Misra [13] for the rounded corner ducts for m_v=60, m_T=70, and ϕ=0.0(a) triangle, (b) square.

Figures 4 (a) through 4 (d) show the variations of fRe_{Dh} with respect to the dimensionless radius

of the rounded corners for the triangular, square, hexagonal, and octagonal ducts, respectively. The results presented in these figures are for ϕ=0.0, 0.01, and 0.02, and for m_v=60. This value of m_v, which has been chosen based on the results of a convergence study, guarantees that fRe_{Dh} converge to a unique value for each of the considered duct cross–sections and for the entire range of the dimensionless radius of the round corners and volume fraction of the nanoparticles presented in Figs. 4 (a) though 4 (d). As it is observed from these figures, irrespective of the magnitude of nanoparticles volume fraction, the minimum values of fRe_{Dh} for each of the considered duct geometries occurs for R_c, i.e., for the corresponding sharp-cornered duct. Moreover, for lower values of R_c, fRe_{Dh} increases rather sharply with increasing R_c for all of the considered polygonal ducts. However, as R_c approaches its maximum possible value in each case, which is essentially equal to the dimensionless radius of the inscribed circle for each of the considered duct geometries, fRe_{Dh} asymptotically approaches the values corresponding to a circular duct. For the base fluid, i.e., for ϕ=0.0, the values of fRe_{Dh} corresponding to the maximum value of R_c is equal to 16.16 which shows excellent agreement with the reported results in the literature [32]. Furthermore, as it is observed from Fig. 4, fRe_{Dh} increases with increasing the nanoparticles volume fraction for all of the considered duct geometries. The resistance to the fluid flow and the pressure drop in the ducts thus increase with increasing the volume fraction of the nanoparticles; however, the velocity profiles remain unchanged. the increase of the friction coefficient with increasing the the volume fraction of the nanoparticles is attributed to the increase of the viscosity of the nanofluid. The viscosity of the nanofluid increases by at most 3 percent as the volume fraction of the nanoparticles increases from ϕ=0.0 to ϕ=0.02. Consequently, as it is demonstrated by Figs. 4 (a) through 4 (d), fRe_{Dh} increases by at most 16 percent as ϕ changes from 0.0 to 0.02.

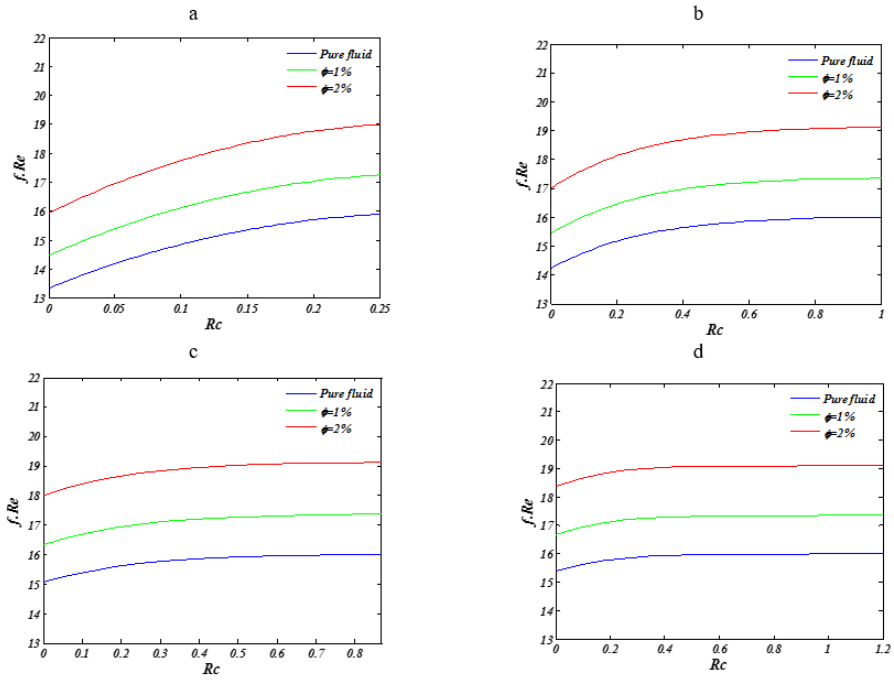

Figure 4: Variation of the converged value of fRe_{Dh} with respect to R_c for different polygonal ducts for m_v=60, ϕ=0.0, 0.01, and 0.02, (a) Triangular, (b) Square, (c) Hexagonal, (d) Octagonal.

Variations of the average Nusselt number of the nanofluid, Nu_{Dh}, with respect to the dimensionless radius of the rounded corners for the triangular, square, hexagonal, and octagonal ducts for the **H1** boundary condition are depicted in Figs. 5 (a) through 5 (d), respectively.

Similar variations for the **T** wall temperature boundary condition are presented in Figs. 6 (a) through 6 (d). The results in these figures are for m_T=70, and for three different nanoparticles volume fractions, namely, ϕ=0.0, 0.01, and 0.02. The convergent velocity profile for each of the polygonal ducts obtained previously is employed to calculate the fully developed temperature profile and the average Nusselt number for the cases presented in Figs. 5 and 6. It is observed from Figs. 5 (a) through 5 (d) and Figs. 6 (a) through 6 (d) that the minimum value of the average Nusselt number, Nu_{Dh}, occurs for R_c=0, i.e., for the sharp cornered ducts, for all of the considered duct cross–sections for both the **H**1 and the **T** wall temperature boundary conditions.

This physically correct behavior is due to the fact that in the non–circular ducts the local heat flux varies from a maximum in wall regions close to the flowing fluid to a minimum in wall regions close to the other wall regions. Consequently, the local heat flux and, in turn, the local Nusselt number decrease significantly near the sharp corners, especially for **T** wall temperature boundary conditions, resulting in a reduction of Nu_{Dh}. Moreover, as the figures show, the average Nusselt number exhibits a steady increase with increasing R_c for all of the considered polygonal ducts and volume fractions of the nanoparticles.

The rate of increase of Nu_{Dh} with respect to R_c is higher for smaller values of the radius of the round corners. Eventually, as R_c approaches its maximum possible value for each case, i.e., the value which corresponds to the radius of the inscribed circle for each of the considered duct cross–sections, the average Nusselt numbers tend asymptotically to the values corresponding to circular ducts; which, for ϕ=0.0, are equal to 4.364 and 3.66 for the uniform heat flux and the isothermal wall boundary conditions, respectively [32]. The average Nusselt numbers for all of the considered cases increase with increasing the volume fraction of the nanoparticles (Figs. 5 and 6). This increases of the average Nusselt number is due to the enhancement of the nanofluid thermal conductivity with increasing ϕ. As ϕ is increased from ϕ=0.0 to ϕ=0.02, the thermal conductivity of the nanofluid and, consequently, the average Nusselt number at most 10 percent (Figs. 5 and 6). Furthermore, as the figures show, the average Nusselt number for the **H1** wall–temperature boundary condition is, in general, substantially larger than that for the **T** wall–temperature boundary condition for all of the considered polygonal ducts and nanoparticles volume fractions.

Based on the results of the current study, new correlations in terms of R_c and ϕ, which are presented in Table 4, are proposed for fRe_{Dh} and Nu_{Dh} for the regular n–sided polygonal ducts with round corners:

5. Conclusion

The Galerkin weighted residuals method is extended to solve the laminar fully developed non–isothermal flow of the Al_2O_3–water nanofluid through the regular n–sided polygonal ducts with round corners. Employing the method, closed–form solutions are obtained for fRe_{Dh} and for the uniform heat flux and the isothermal wall temperature boundary conditions in terms of the radius of the round corner and volume fraction of the nanoparticle. Comparisons of the results with those existing in the literature for the triangular and square ducts with round corners for the uniform heat flux boundary condition show very good agreements between them. The main conclusions are summarized below:

- fRe_{Dh} increases with increasing the radius of the round corners for all the considered duct cross–sections.
- The rate of increase if the friction coefficient with respect to R_c decreases with increasing the number of sides of polygonal ducts.

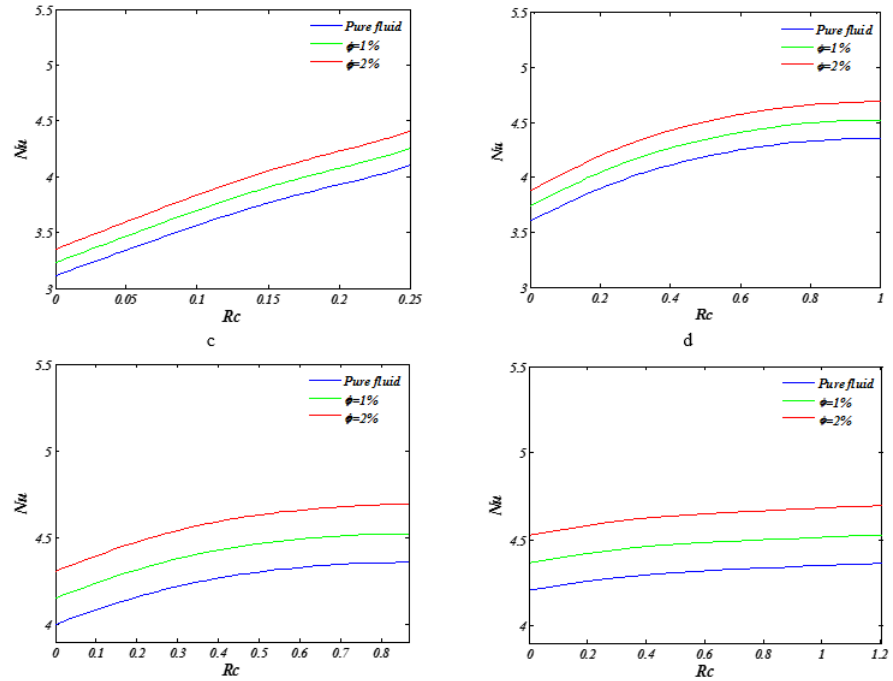

Figure 5: Variation of the average Nusselt number with respect to $R_c$for different polygonal ducts for the **H1** wall temperature boundary condition, m_T=70,ϕ=0.0, 0.01, and 0.02, (a) Triangular, (b) Square, (c) Hexagonal, (d) Octagonal.

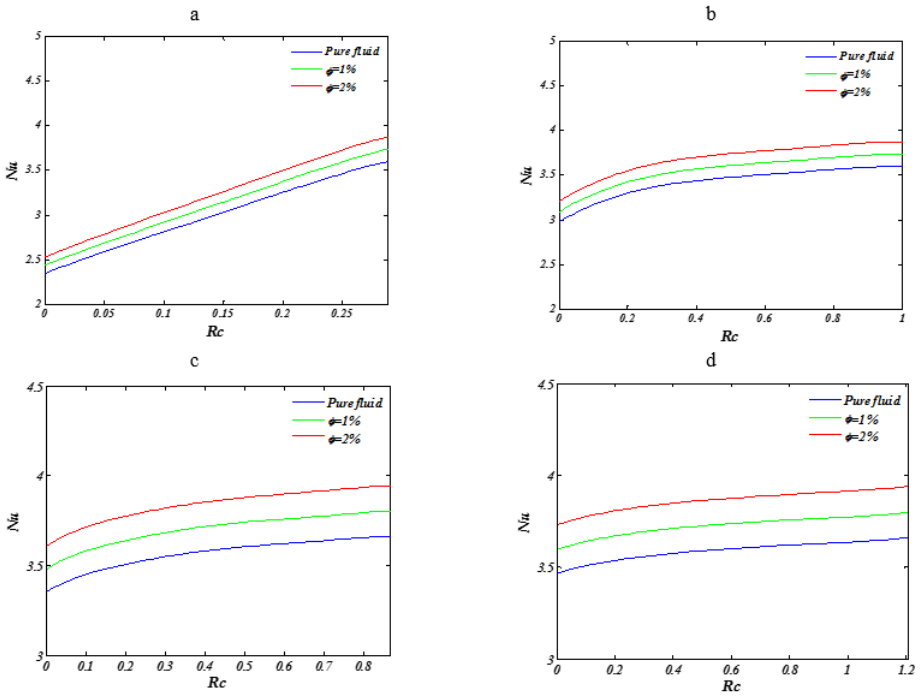

Figure 6: Variation of the average Nusselt number with respect to $R_c$for different polygonal ducts for the **T** wall temperature boundary condition, m_T=70,ϕ=0.0, 0.01, and 0.02, (a) Triangular, (b) Square, (c) Hexagonal, (d) Octagonal

Table 4: fRe_{Dh} and Nu_{Dh} correlations for the regular n-sided polygonal ducts with round corners

Triangular		$f\,\mathrm{Re} = [123\phi^2 + 7.3\phi + 1]\,[15.504R_c^5 - 40.522R_c^4 + 32.882R_c^3 - 40.953R_c^2 + 19.025R_c + 13.333]$
	H1	$Nu_{Dh} = \frac{k_p+2k_{bf}+2\phi\left(k_p-k_{bf}\right)(1+\beta)^3}{k_p+2k_{bf}-\phi\left(k_p-k_{bf}\right)(1+\beta)^3}$
		$[1426.4R_c^5 - 693.77R_c^4 + 98.554R_c^3 - 6.9483R_c^2 + 4.804R_c + 3.1144]$
	T	$Nu_{Dh} = \frac{k_p+2k_{bf}+2\phi\left(k_p-k_{bf}\right)(1+\beta)^3}{k_p+2k_{bf}-\phi\left(k_p-k_{bf}\right)(1+\beta)^3}$
		$[-141.38R_c^5 + 3.9659R_c^4 + 26.977R_c^3 - 7.2928R_c^2 + 5.0799R_c + 2.3521]$
Square		$f\mathrm{Re}_{Dh} = [123\phi^2 + 7.3\phi + 1]\,[5.54R_c^6 - 16.34R_c^5 + 16.11R_c^4 - 2.45R_c^3 - 7.22R_c^2 + 6.14R_c + 14.23]$
	H1	$Nu_{Dh} = \frac{k_p+2k_{bf}+2\phi\left(k_p-k_{bf}\right)(1+\beta)^3}{k_p+2k_{bf}-\phi\left(k_p-k_{bf}\right)(1+\beta)^3}$
		$[4.8873R_c^6 - 15.444R_c^5 + 18.523R_c^4 - 10.187R_c^3 + 1.5304R_c^2 + 1.4403R_c + 3.6092]$
	T	$Nu_{Dh} = \frac{k_p+2k_{bf}+2\phi\left(k_p-k_{bf}\right)(1+\beta)^3}{k_p+2k_{bf}-\phi\left(k_p-k_{bf}\right)(1+\beta)^3}$
		$[-0.87059R_c^5 + 0.64711R_c^4 + 2.3204R_c^3 - 3.7246R_c^2 + 2.2483R_c + 2.9787]$
Hexagonal		$f\mathrm{Re}_{Dh} = [123\phi^2 + 7.3\phi + 1]\,[-1.6387Rc^4 + 5.363Rc^3 - 6.687Rc^2 + 3.9222Rc + 15.06]$
	H1	$Nu_{Dh} = \frac{k_p+2k_{bf}+2\phi\left(k_p-k_{bf}\right)(1+\beta)^3}{k_p+2k_{bf}-\phi\left(k_p-k_{bf}\right)(1+\beta)^3}$
		$[-0.2822Rc^6 - 0.3512Rc^5 + 1.8801Rc^4 - 1.7205Rc^3 - 0.0359Rc^2 + 0.8484Rc + 4.0021]$
	T	$Nu_{Dh} = \frac{k_p+2k_{bf}+2\phi\left(k_p-k_{bf}\right)(1+\beta)^3}{k_p+2k_{bf}-\phi\left(k_p-k_{bf}\right)(1+\beta)^3}$
		$[-10.23Rc^6 + 27.994Rc^5 - 29.927Rc^4 + 16.283Rc^3 - 5.2587Rc^2 + 1.3743Rc + 3.3532]$
Octagonal		$f\mathrm{Re}_{Dh} = [123\phi^2 + 7.3\phi + 1]\,[-1.33Rc^4 + 4.478Rc^3 - 5.481Rc^2 + 2.941Rc + 15.38]$
	H1	$Nu_{Dh} = \frac{k_p+2k_{bf}+2\phi\left(k_p-k_{bf}\right)(1+\beta)^3}{k_p+2k_{bf}-\phi\left(k_p-k_{bf}\right)(1+\beta)^3}$
		$[-0.2992Rc^5 + 0.9112Rc^4 - 0.8723Rc^3 + 0.1458Rc^2 + 0.2578Rc + 4.207]$
	T	$Nu_{Dh} = \frac{k_p+2k_{bf}+2\phi\left(k_p-k_{bf}\right)(1+\beta)^3}{k_p+2k_{bf}-\phi\left(k_p-k_{bf}\right)(1+\beta)^3}$
		$[0.23381R_c^5 - 0.78527R_c^4 + 1.1048R_c^3 - 0.87232R_c^2 + 0.48785R_c + 3.4677]$

- The average Nusselt number, Nu_{Dh}, increases with increasing R_c for all of the considered duct cross-sections.
- The rate of increase of Nu_{Dh} with respect to R_c decreases with increasing the number of sides of the polygonal ducts.
- fRe_{Dh} and Nu_{Dh} advance asymptotically toward the values for a circular duct as R_c approaches its maximum value for each of the duct cross–sections and for both the **H1** and **T** boundary conditions.
- The rate of increase of fRe_{Dh} and Nu_{Dh} with respect to R_c are initially quite large and decrease as R_c increases
- fRe_{Dh} and Nu_{Dh} increase with increasing the volume fraction of nanoparticles for all of the considered cases.
- Novel correlations for fRe_{Dh} and Nu_{Dh} in terms of the dimensionless radius of the round corners and the volume fraction of the nanoparticles are presented for the n-sided regular polygonal ducts for the uniform heat flux and isothermal wall temperature boundary conditions.

Close agreements of the obtained results with those existing in the literature for the triangular and square ducts with round corners for the constant heat flux boundary condition as well as the capability of the method to provide physically correct new results for various polygonal ducts with round corners for both constant heat flux and constant wall temperature boundary conditions indicate that the Galerkin weighted residual method is quite promising for obtaining closed-form solutions for the flow and heat transfer of nanofluid in domains with complex geometries.

References

[1] E.M. Sparrow and R. Siegel, *A variational method for fully developed laminar heat transfer in ducts*, Transaction of ASME, J. Heat Transf., 81 (1959) 157–167.

[2] E.M. Sparrow and A.L. Loeffler , *Longitudinal laminar flow between cylinders arranged in regular array.* AIChE J., 5 (1959) 325–330..

[3] E.M. Sparoow, A.L. Loeffler and H.A. Hubbard, *Heat transfer to longitudinal laminar flow between cylinders*, Transaction of ASME, J. Heat Transfer, 83 (1961) 415–422.

[4] K.C. Cheng and M. Jamil, *Laminar flow and heat transfer in circular ducts with diametrically opposite flat sides and ducts of multiply connected cross sections*, Can. J. Chem. Eng., 48 (1970) 333–334.

[5] E.M. Sparrow and A. Haji-Sheikh, *Flow and heat transfer in ducts of arbitrary shape with arbitrary thermal boundary conditions*, J. Heat Transfer, 88 (1966) 351–357.

[6] D.A. Ratkowsky and N. Epstein, *Laminar flow in regular polygonal shaped ducts with circular centered cores.* J. Chem. Eng., 46 (1968) 22–26.

[7] R. Shah, *Laminar flow friction and forced convection heat transfer in ducts of arbitrary geometry.* Int. J. Heat and Mass Transfer, 18 (1975) 849–862.

[8] G.H. Golub, *Numerical methods for solving linear least-squares problem*, Numer. Math., 7 (1965) 206–216.

[9] A. Haji-Sheikh, M. Mashena and M.J. Haji-Sheikh, *Heat transfer coefficients in ducts with constant wall temperature*, J. Heat Transfer, 105 (1983) 878.

[10] Y.M. Lee and Y.M. Kuo, *Laminar Flow in annuli ducts with constant wall temperature*, Transf., 25 (1998) 227–236.

[11] Y.M. Lee and P.C. Lee, *Laminar Flow in elliptic ducts with and without central circular cores for constant wall temperature*, Int. Commun. Heat Mass Transf., 28 (2001) 1115–1124.

[12] S. Tahernejad Ledari, H.H. Mirgolbabaee, D. Domiri Ganji, *An assessment of a semi analytical AG method for solving two-dimension nonlinear viscous flow*, Int. J. Nonlinear Anal. Appl., 6 (2015) 47–64.

[13] S. Ray and D. Misra, *Laminar fully developed flow through square and equilateral triangular ducts with rounded corners subjected to H1 and H2 boundary conditions*, Int. J. Therm. Sci., 49 (2010) 1763–1775.

[14] S. Shahsavari, A. Tamayol, E. Kjeang and M. Bahrami, *Convective heat transfer in microchannels of noncircular cross sections: An analytical approach*, J. Heat Transfer, 134 (2012) 091701.

[15] F. Schmidt and M. Newell, *Heat transfer in fully developed laminar ow through rectangular and isosceles triangular ducts*, Int. J. Heat Mass Transf., 10 (1967) 1121–1123.

[16] A. Yutaka, N. Hiroshi and M. Faghri, *Developing laminar ow and heat transfer in the entrance region of regular polygonal ducts*, Int. J. Heat Mass Transf., 31 (1988) 2590–2593.

[17] S. Syrjal, *Further*
finite element analyses of fully developed laminar flow of power-law non-Newtonian fluid in rectangular ducts: Heat transfer predictions, Int. Commun. Heat Mass Transf., 23 (1996) 799–807.

[18] M. Mahadevappa, V. Rammohan Rao and V. Sastri, *Numerical study of steady laminar fully developed fluid flow*, Int. J. Heat and Mass Transfer, 39 (1996) 867–875.

[19] R.J. Silva, R.M. Valle and M. Ziviani, *Numerical hydrodynamic and thermal analysis of laminar flow in curved elliptic and rectangular ducts*, Int. J. Therm. Sci., 38 (1999) 585–594.

[20] R. Sadasivam, R.M. Manglik and M.A. Jog, *Fully developed forced convection through trapezoidal and hexagonal ducts*, Int. J. Heat Mass Transf., 42 (1999) 4321–4331.

[21] A. Arefmanesh and M. Abbaszadeh, *On the Natural Stabilization of Convection Diffusion Problems Using LPIM Meshless Method*, Int. J. Nonlinear Anal. Appl., 8 (2017) 9–22.

[22] S. Singh, D. Kumar, K.N. Rai and M.A. Jog, *Wavelet collocation solution of non-linear Fin problem with temperature dependent thermal conductivity and heat transfer coefficient*, Int. J. Nonlinear Anal. Appl., 6 (2014) 105–118.

[23] O. Turgut, *Numerical investigation of laminar flow and heat transfer in hexagonal ducts under isothermal and constant heat flux boundary conditions*, J. Sci. Technol. Trans. Mech. Eng., 38 (2014) 45–56.

[24] M.S.Y. Ebaid, O.M.Haddad and L.R. Batarseh, *Numerical investigation of fully developed laminar flow in irregular annular ducts: Triangular-circular combinations*, Enery Conver. Manag., 85 (2014) 511–520.

[25] S. Zeinali Heris, M. Nasr Esfahany and S. Etemad, *Experimental investigation of convective heat transfer of Al2O3-water nanofluid in circular tube*, Int. J. Heat Fluid Flow, 28 (2007) 203–210.

[26] R.S. Vajjha, D.K. Das and P.K. Namburu, *Numerical study of fluid dynamic and heat transfer performance of Al2O3 and CuO nanofluids in the flat tubes of a radiator*, Int. J. Heat Fluid Flow, 31 (2010) 613–621.

[27] T.H. Nassan, S.Z. Heris and S. Noie, *A comparison of experimental heat transfer characteristics for Al2O3-water and CuO-water nano uids in square cross-section duct*, Int. Commun. Heat Mass Transfer, 37 (2010) 924–928.

[28] P. Kumar, *A CFD Study of Heat Transfer Enhancement in Pipe Flow with Al2O3 Nanofluid*, World Academy of Science, Eng. Tech., 5 (2011) 746–750.
[29] M. Nasiri, S. Etemad, R. Bagheri, *Experimental heat transfer of nanofluid through an annular duct*, Int. Commun. Heat Mass Transfer, 38 (2011) 958–963.
[30] S. Zeinali Heris, T.H. Nassan, S. Noie, H. Sardarabadi and M. Sardarabadi, *Laminar convective heat transfer of Al2O3/water nanofluid through square cross-sectional duct*, Int. J. Heat Fluid Flow, 44 (2013) 375-–382.
[31] H.K. Dawood, H.A. Mohammed and K.M. Munisamy, *Heat transfer augmentation using nanofluids in an elliptic annulus with constant heat flux boundary condition*, Case Studies Therm. Eng., 4 (2014) 32-–41.
[32] A. Bejan, *Convection Heat Transfer*, John Wiley and Sons, Inc., Hoboken, NJ, USA, 2013.
[33] K. Khanafer and K. Vafai, *A critical synthesis of thermophysical characteristics of nanofluids*, Int. J. Heat Mass Transfer, 54 (2011) 4410–4428.
[34] A. Arefmanesh, A. Aghaei and H. Ehteram, *Mixed convection heat transfer in a CuOwater filled trapezoidal enclosure,effects of various constant and variable properties of the nanofluid*, Appl. Math. Model., 40 (2016) 815–831.
[35] W. Yu and S. Choi, *The role of interfacial layers in the enhanced thermal conductivity of nanofluids: a renovated Maxwell model*, J. Nanoparticle Res., 5 (2003) 167–171.
[36] S.E.B. Maiga, S.J. Palm, C.T. Nguyen, G. Roy and N. Galanis, *Heat transfer enhancement by using nanofluids in forced convection flows*, Int. J. Heat Fluid Flow, 26 (2005) 530–546.